

Autonomous Three-Dimensional Formation Flight for a Swarm of Unmanned Aerial Vehicles

Derek J. Bennet* and C. R. McInnes†

University of Strathclyde, Glasgow, Scotland, G1 1XJ, United Kingdom
 and

M. Suzuki‡ and K. Uchiyama§

Nihon University, Funabashi 274-8501, Japan

DOI: 10.2514/1.53931

This paper investigates the development of a new guidance algorithm for a formation of unmanned aerial vehicles. Using the new approach of bifurcating potential fields, it is shown that a formation of unmanned aerial vehicles can be successfully controlled such that verifiable autonomous patterns are achieved, with a simple parameter switch allowing for transitions between patterns. The key contribution that this paper presents is in the development of a new bounded bifurcating potential field that avoids saturating the vehicle actuators, which is essential for real or safety-critical applications. To demonstrate this, a guidance and control method is developed, based on a six-degree-of-freedom linearized aircraft model, showing that, in simulation, three-dimensional formation flight for a swarm of unmanned aerial vehicles can be achieved.

Nomenclature

a, b, c	= formation control constants	\mathbf{v}_i^R	= repulsive velocity vector of the i th unmanned aerial vehicle
C_e, L_e	= exponential potential amplitude and length scale	\mathbf{v}_i^S	= steering velocity vector of the i th unmanned aerial vehicle
C_h	= hyperbolic amplitude	$\mathbf{v}_i^{S,e}$	= exponential steering velocity vector of the i th unmanned aerial vehicle
C_r, L_r	= repulsive potential amplitude and length scale	$\mathbf{v}_i^{S,h}$	= hyperbolic steering velocity vector of the i th unmanned aerial vehicle
\mathbf{e}	= error in system	\mathbf{x}_i	= position vector of the i th unmanned aerial vehicle
$\mathbf{K}_1, \mathbf{K}_2$	= controller feedback gains	\mathbf{x}_j	= position vector of the j th unmanned aerial vehicle
N	= number of unmanned aerial vehicles	$\bar{\mathbf{x}}_{\text{lat}}$	= lateral state variables
p, q, r	= roll, pitch, and yaw rates, rad/s^{-1}	$\bar{\mathbf{x}}_{\text{long}}$	= longitudinal state variable
r	= scalar constant	\mathbf{x}_o	= equilibrium position vector
u, v, w	= body axis speed in $x, y,$ and z directions, ms^{-1}	\mathbf{y}	= output of control system
u_d	= desired unmanned-aerial-vehicle speed, m/s	\mathbf{y}_d	= desired input to the system
\mathbf{u}_{lat}	= lateral inputs	$\delta_e, \delta_a, \delta_r$	= input to elevator, aileron, and rudder, rad
\mathbf{u}_{long}	= longitudinal inputs	$\delta_{e,d}, \delta_{a,d}, \delta_{r,d}$	= desired input to elevator, aileron, and rudder, rad
u_x	= desired unmanned-aerial-vehicle forward speed, m/s	δ_r	= thrust input, N
$U_i^{S,e}$	= exponential steering potential of the i th unmanned aerial vehicle	$\delta_{r,d}$	= desired thrust input, N
$U_i^{S,h}$	= hyperbolic steering potential of the i th unmanned aerial vehicle	θ_d	= desired pitch angle, rad
$U_i^{S,he}$	= combined hyperbolic-exponential steering potential of the i th unmanned aerial vehicle	μ	= bifurcation parameter
U^R	= repulsive potential field	σ_i	= formation control scalar
U^S	= steering potential field	ϕ, θ, ψ	= roll, pitch, and yaw angles, rad
V_{max}	= maximum speed of the unmanned aerial vehicle	ψ_d	= desired heading angle, rad
V_{trim}	= trim speed of the unmanned aerial vehicle	(\cdot)	= unit vector
\mathbf{v}_i	= velocity vector of i th unmanned aerial vehicle		
\mathbf{v}_j	= velocity vector of j th unmanned aerial vehicle		

Presented as Paper 2009-5884 at the AIAA Guidance, Navigation, and Control Conference, Chicago, IL, 10–13 August 2009; received 11 February 2011; revision received 11 May 2011; accepted for publication 25 May 2011. Copyright © 2011 by the American Institute of Aeronautics and Astronautics, Inc. All rights reserved. Copies of this paper may be made for personal or internal use, on condition that the copier pay the \$10.00 per-copy fee to the Copyright Clearance Center, Inc., 222 Rosewood Drive, Danvers, MA 01923; include the code 0731-5090/11 and \$10.00 in correspondence with the CCC.

*Teaching Fellow, Department of Mechanical Engineering; derek.bennet@strath.ac.uk.

†Professor, Department of Mechanical Engineering; colin.mcinnis@strath.ac.uk.

‡Graduate Student, Department of Aerospace Engineering; csms09015@g.nihon-u.ac.jp

§Associate Professor, Department of Aerospace Engineering; uchiyama@aero.cst.nihon-u.ac.jp. Senior Member AIAA.

I. Introduction

IN RECENT years, the area of swarm robotics has developed into a major research field driven by the need to solve engineering problems in new and efficient ways. A key aspect of the swarm system is that it is distributed and therefore does not rely on a central controller. Consequently, these systems can have the advantages of being robust, scalable, and flexible, and they allow engineers the opportunity to approach problems in new ways.

One of the areas researching swarm robotics is the control of formations of unmanned aerial vehicles (UAVs) [1–6]. The potential applications for this type of system are for scientific data gathering or for military convoy protection, for example. To control these systems, researchers often base the development of the control architectures on the swarm intelligence paradigm that describes “any attempt to design algorithms or distributed problem-solving devices inspired by the collective behavior of social insect colonies and other animal societies” [7].

One of the first to implement this idea was Reynolds's boids simulation of flocking in birds in 1987 [8]. This heuristic ruled-based approach based the movement of each boid on three simple steering behaviors (separation, alignment, and cohesion) and produced interesting qualitative behaviors. The method was later investigated by Heppner and Grenander [9] and more recently applied to formation control of autonomous UAVs by Crowther [10,11]. Although producing successful behaviors, demonstrating that swarming behavior can be replicated through a set of simple rules, this approach lacks formal verification for the behaviors, and therefore limits its ability to be applied to a real engineered system.

In the mid-1980s, Brooks introduced a paradigm shift in the way that robotic systems were designed [12]. Compared with the traditional artificial intelligence approach that aimed at reproducing human cognition, Brooks developed a behavior-based approach that did not require an internal model of the environment, creating a completely reactive system driven by sensing and communication. The algorithm developed was the subsumption architecture that consists of a layered set of behaviors with top-level behaviors subsuming lower-level behaviors. A related approach is finite state automata, where robots are modeled as finite state machines with the use of Markov dynamics to describe the behavior of the swarm [13]. Both of these ad hoc approaches successfully produced interesting qualitative behaviors such as flocking and dispersion; however, they also had no formal means of verification.

The artificial potential field (APF) method is a fusion behavior-based architecture that combines several behaviors together, resulting in a superimposed behavior. It was first introduced by Khatib [14] in the area of obstacle avoidance for manipulators and mobile robots and has been studied extensively for autonomous path planning for single mobile robots [15–18] and more recently has been applied to autonomous swarming systems [19–22]. The APF field is used to generate a first- or second-order dynamical system and can often be used to mathematically prove the stability of the emergent behaviors, therefore replacing traditional algorithm validation. In addition, there exists an array of theorems in dynamical systems theory that can be used to develop new ways of controlling a swarm.

In [23], it was shown that by using a steering and repulsive APF, a swarm of UAVs can be successfully controlled such that desired patterns are formed, with the new approach of bifurcating potential fields allowing for a transition between different patterns through a simple parameter switch. Using a first-order dynamical system, the desired swarm velocity field is transformed into guidance commands for forward control speed and heading angle. This paper extends the analysis by developing a bounded bifurcating potential field. To prevent the guidance velocity command from becoming saturated, a bounded bifurcating hyperbolic potential is introduced. In addition, the APF is generalized so that the swarm can be attracted to a variety of different states. To demonstrate the model, the guidance algorithm is applied to a formation of nine fixed-wing UAVs, considering a linearized six-degree-of-freedom (6-DOF) UAV model, with a robust controller designed for the linear time-invariant multivariable systems used.

Related work on the use of the APF method to control UAVs includes Frew et al., who implemented Lyapunov vector fields for the guidance of unmanned aircraft [24]. They showed that this approach provides a globally stable convergence to a limit-cycle behavior for a single UAV platform and verified the simulation result in the development of a real UAV. In addition, Han et al. implemented the APF and a robust sliding mode controller in order to simulate the control of a swarm of UAVs, showing that their proposed method of a swarm geometry center control can track a desired trajectory [25].

The paper proceeds as follows. In the next section, a new bound bifurcating potential field is developed and then generalized so that different UAV swarm patterns can be achieved. The new guidance algorithm is then applied to a swarm of nine UAVs, considering a 6-DOF linearized UAV model. Under the assumption that the longitudinal and lateral aircraft equations of motion can be decoupled, it is shown that the UAVs can form different autonomous patterns, following the desired commands.

II. Swarm Unmanned-Aerial-Vehicle Model

A. Velocity Field

A swarm of N homogeneous UAVs are considered, where $(\mathbf{x}_i, \mathbf{v}_i)$ and $(\mathbf{x}_j, \mathbf{v}_j)$ define the position and velocity vectors of the i th and j th UAVs, respectively, and \mathbf{x}_{ij} defines the separation distance between the i th and j th UAVs, as shown in Fig. 1.

Each UAV is treated as a particle, acted upon by a velocity field as described in Eq. (1):

$$\mathbf{v}_i = -\nabla_i U^S(\mathbf{x}_i) - \nabla_i U^R(\mathbf{x}_{ij}) \quad (1)$$

where U^S and U^R are defined as the steering and repulsive APFs, respectively, $\mathbf{x}_i = (x_i, y_i, z_i)^T$ and $\mathbf{x}_{ij} = \mathbf{x}_i - \mathbf{x}_j$.

As can be seen in Eq. (1), the gradient of the steering and repulsive potential defines a velocity field acting on each UAV, where the steering potential is used to control the formation and the repulsive potential is used for collision avoidance and an equally spaced final formation.

B. Artificial Potential Field

Related previous work has shown that by using a guidance algorithm, based on classical bifurcation theory, a formation of UAVs can create autonomous desired patterns, switching between patterns through a simple parameter change [23]. Using Lyapunov stability methods, the desired autonomous patterns can be analytically proven as opposed to traditional algorithm validation methods. To ensure the stability of real safety or mission critical systems, it is important to consider the issue of saturation. A new bounded bifurcating potential field is therefore developed. Considering Eq. (1), it can be seen that through the triangle inequality, the maximum control velocity for the i th UAV is

$$|\mathbf{v}_i| \leq |\nabla_i U^S(\mathbf{x}_i)| + |\nabla_i U^R(\mathbf{x}_{ij})| \quad (2)$$

Therefore, the maximum control velocity each UAV will experience is a combination of the maximum gradient of the steering and repulsive potentials.

1. Bifurcating Steering Potential

Bifurcating potential fields allow for the manipulation of the shape of the potential through a simple parameter change. This change alters the stability properties of the potential, and thus the emergent patterns that the swarm relaxes into. An example of bifurcating steering potential is shown in Eq. (3) based on the pitchfork bifurcation equation:

$$U_i^S(\mathbf{x}_i; \mu) = -\frac{1}{2}\mu(|\mathbf{x}_i| - r)^2 + \frac{1}{4}(|\mathbf{x}_i| - r)^4 \quad (3)$$

where μ is the bifurcation parameter, and r is a scalar.

Figures 2 and 3 show how the potential and number of equilibrium positions alter as the bifurcation parameter is changed. As can be seen, if $\mu < 0$, there is one stable equilibrium position; however, if $\mu > 0$, there are then two stable equilibrium positions.

As stated in Eq. (1), the gradient of the potential defines a velocity field acting on each UAV. Therefore, Eq. (4) and Fig. 4 show the velocity field \mathbf{v}_i^S due to the pitchfork potential:

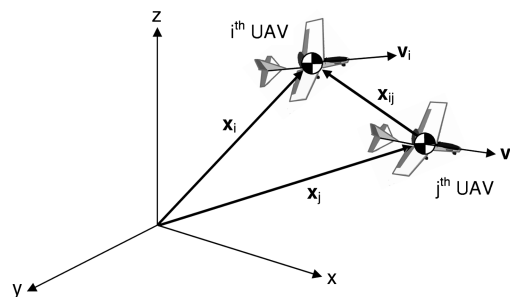


Fig. 1 Definition of UAV position and velocity vectors.

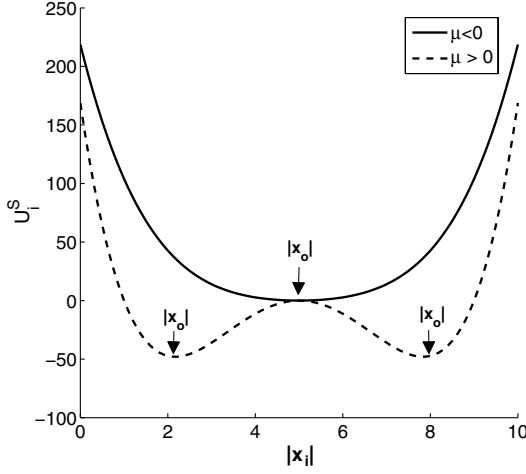


Fig. 2 Pitchfork potential, $r = 5$ ($|x_o|$ denotes equilibrium position).

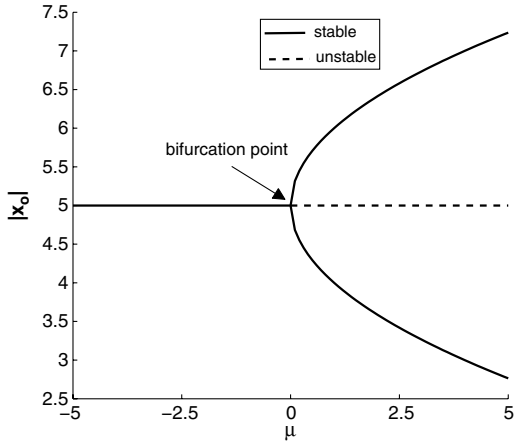


Fig. 3 Pitchfork bifurcation diagram, $r = 5$.

$$\mathbf{v}_i^S = -\nabla_i U^S(\mathbf{x}_i) = [\mu(|\mathbf{x}_i| - r) - (|\mathbf{x}_i| - r)^3] \hat{\mathbf{x}}_i \quad (4)$$

where $\hat{(\cdot)}$ denotes a unit vector.

As can be seen from Eq. (4) and Fig. 4, the steering control velocity is unbound as distance from the equilibrium position increases; therefore, the issue of velocity saturation may occur in a real system.

To overcome this problem, a hyperbolic potential field can be used, as proposed by Badawy and McInnes [26]. This function has a bound, constant gradient as the distance from the equilibrium position increases and has a smooth shape at the goal. Equation (5)

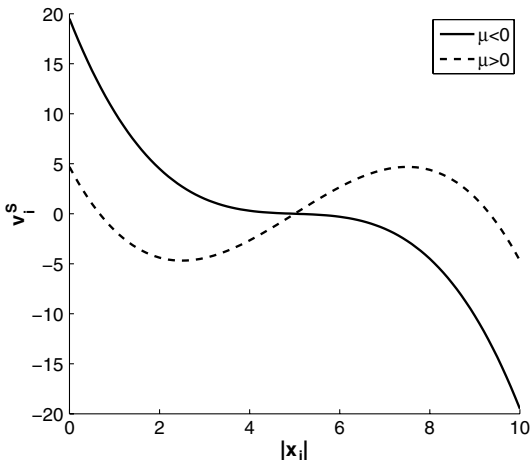


Fig. 4 Pitchfork steering potential velocity, $r = 5$.

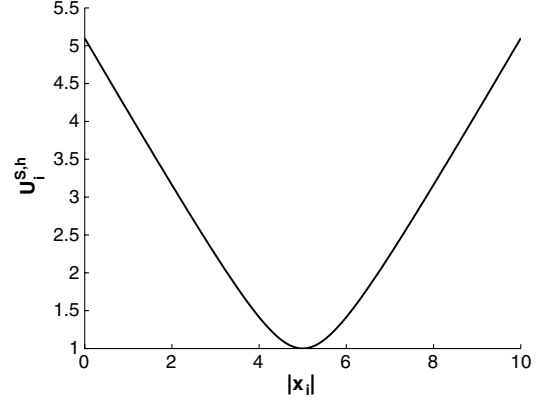


Fig. 5 Hyperbolic potential function ($C_h = 1$).

and Fig. 5 show the hyperbolic potential field $U_i^{S,h}(\mathbf{x}_i)$ that can be used to steer the UAVs:

$$U_i^{S,h}(\mathbf{x}_i) = C_h[(|\mathbf{x}_i| - r)^2 + 1]^{0.5} \quad (5)$$

where C_h controls the amplitude of this function.

To achieve a bifurcating potential field, an additional exponential steering potential term is added, as shown in Eq. (6) and Fig. 6:

$$U_i^{S,e}(\mathbf{x}_i) = \mu C_e \exp[-(|\mathbf{x}_i| - r)^2 / L_e] \quad (6)$$

where C_e and L_e control the amplitude and range of the potential, respectively, and μ is the bifurcation parameter.

Combining Eqs. (5) and (6) results in a bound steering potential $U_i^{S,he}(\mathbf{x}_i)$ given in Eq. (7) and Fig. 7. Again, if $\mu < 0$, there is one equilibrium position; however, if $\mu > 0$, the potential will bifurcate into two stable equilibrium positions:

$$U_i^{S,he}(\mathbf{x}_i) = C_h[(|\mathbf{x}_i| - r)^2 + 1]^{0.5} + \mu C_e \exp[-(|\mathbf{x}_i| - r)^2 / L_e] \quad (7)$$

The maximum value of the new bound velocity field can be found analytically. First, consider the hyperbolic potential function given in Eq. (5). The velocity $\mathbf{v}_i^{S,h}$ due to this term is given in Eq. (8) and Fig. 8:

$$\mathbf{v}_i^{S,h} = -\nabla_i U^{S,h}(\mathbf{x}_i) = -\frac{C_h(|\mathbf{x}_i| - r)}{[(|\mathbf{x}_i| - r)^2 + 1]^{0.5}} \hat{\mathbf{x}}_i \quad (8)$$

Therefore, the maximum velocity due to this term is

$$|\mathbf{v}_i^{S,h}|_{\max} = C_h \quad (9)$$

Next, consider the exponential steering potential given in Eq. (6). The velocity $\mathbf{v}_i^{S,e}$ due to this term is given in Eq. (10) and Fig. 9:

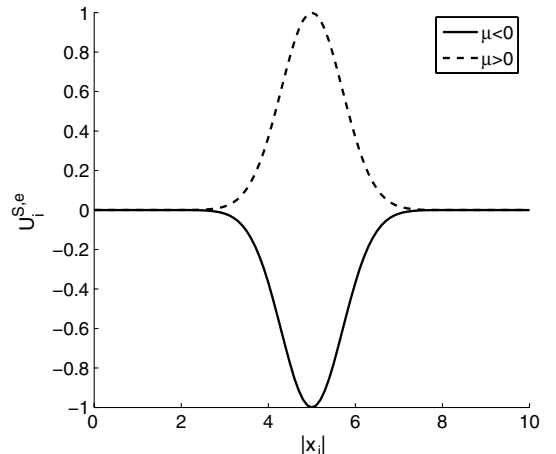


Fig. 6 Exponential potential function ($C_e = 1, L_e = 1$, and $r = 5$).

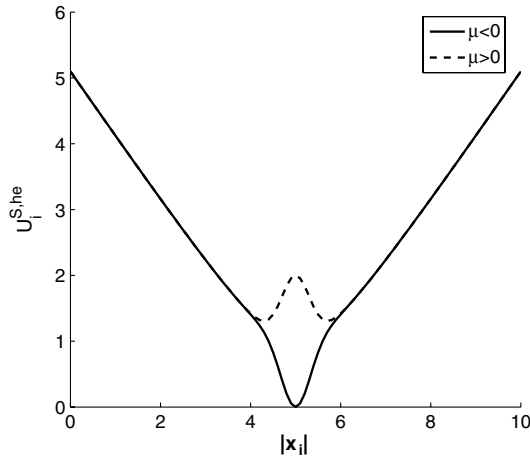


Fig. 7 Combined bound bifurcating potential function ($C_h = 1$, $C_e = 1$, $L_e = 0.2$, and $r = 5$).

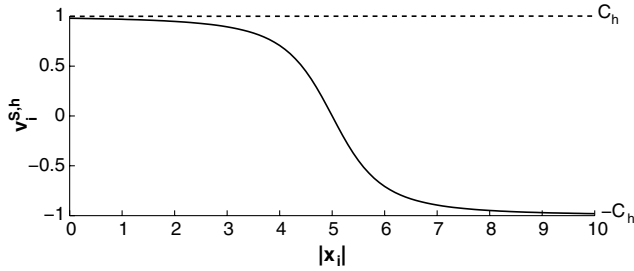


Fig. 8 Velocity due to hyperbolic term ($C_h = 1$).

$$\mathbf{v}_i^{S,e} = -\nabla_i U^{S,e}(\mathbf{x}_i) = 2\mu \frac{C_e}{L_e} \hat{\mathbf{x}}_i (|\mathbf{x}_i| - r) \exp^{-[(|\mathbf{x}_i| - r)^2 / L_e]} \quad (10)$$

The maximum velocity due to the exponential term $|\mathbf{v}_i^{S,e}|_{\max}$ occurs when $|\mathbf{x}_i| = r \pm \sqrt{L_e/2}$, giving

$$|\mathbf{v}_i^{S,e}|_{\max} = \sqrt{2}\mu \exp^{-0.5} \frac{C_e}{\sqrt{L_e}} \quad (11)$$

Depending upon the constants chosen in Eq. (7), the maximum bound velocity will either be controlled through the hyperbolic or exponential term. Figure 10 illustrates this for the case when $\mu > 0$, and constants are chosen so that either the hyperbolic or exponential term dominates. If the hyperbolic term dominates, $|\mathbf{v}_i^{S,he}|_{\max} = C_h$. If, however, the exponential term dominates, then $|\mathbf{v}_i^{S,he}|_{\max}$ can be found numerically.

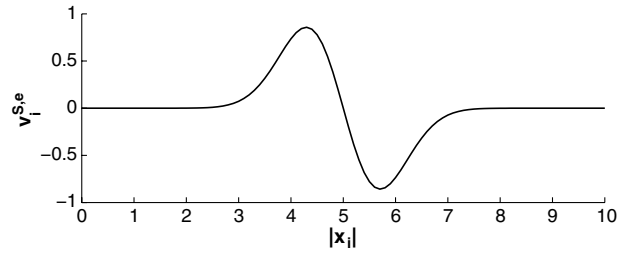


Fig. 9 Velocity due to exponential term ($\mu = -1$, $C_e = 1$, $L_e = 0.2$, and $r = 5$).

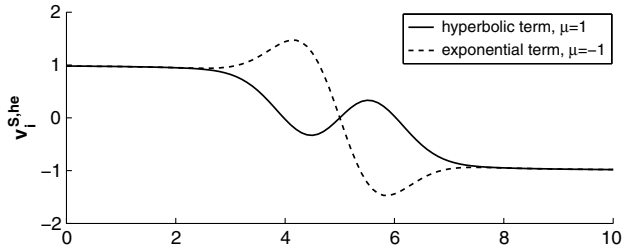


Fig. 10 Bound bifurcating velocity ($C_h = 1$, $C_e = 1$, $L_e = 1$, and $r = 5$).

2. Repulsive Potential

The repulsive potential is a simple pairwise exponential function that is based on a generalized Morse potential [22] as follows

$$U_i^R = \sum_{j:j \neq i} C_r \exp^{-|\mathbf{x}_{ij}|/L_r} \quad (12)$$

where $|\mathbf{x}_{ij}| = |\mathbf{x}_i - \mathbf{x}_j|$ and C_r and L_r are constants controlling the amplitude and length scale of the potential, respectively.

The repulsive potential is a bound velocity that has a maximum value equal to C_r/L_r that occurs when $\mathbf{x}_{ij} = 0$. This would, however, occur when two UAVs are in the same position, and therefore would have collided. The realistic maximum control velocity can therefore be expressed as

$$|\mathbf{v}_i^R|_{\max} = C_r/L_r \exp^{-(|\mathbf{x}_{ij}|_{\min}/L_r)} \quad (13)$$

where $|\mathbf{x}_{ij}|_{\min} = |\mathbf{x}_i - \mathbf{x}_j|_{\min}$ is the minimum separation distance between both UAVs without colliding, as shown in Fig. 11, for example.

III. Pattern Formation and Reconfigurability

To allow three-dimensional formation patterns, the following steering potential can be used based on the bound bifurcating potential discussed in the previous section:

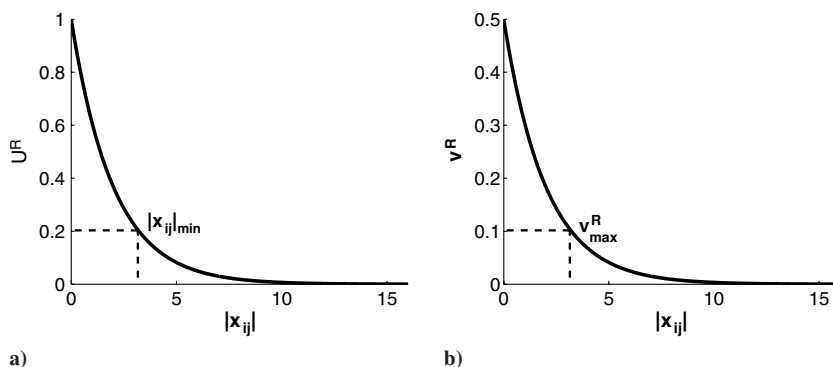


Fig. 11 Repulsive potential field ($C_r = 1$, $L_r = 2$): a) potential field and b) control velocity.

Table 1 Formation free parameters

Formation	Time, s	μ	r	C_r	L_r	C_h	C_e	L_e	a	b	c	u_x
A	0–50	2	4	10	1	1	1.5	1.5	1	0	0	1
B	50–100	-1	6	10	1	1	1.5	1.5	1	0	0	1
C	100–150	-1	6	10	1	1	1.5	1.5	0	0	1	1

$$U^S(\mathbf{x}_i) = C_h[\sqrt{(|\mathbf{x}_i| - r)^2 + 1} + \sqrt{\sigma_i^2 + 1}] + \mu C_e \exp\left(-\frac{(|\mathbf{x}_i| - r)^2}{L_e}\right) \quad (14)$$

where

$$|\mathbf{x}_i| = \sqrt{(x_i^2 + y_i^2 + z_i^2)} \quad (15)$$

$$\sigma_i = \mathbf{k} \cdot \mathbf{x}_i \quad (16)$$

$$\mathbf{k} = (a, b, c)^T \quad (17)$$

and a , b , and c are constants.

The purpose of this steering potential is to drive the UAVs to a distance r from the origin, with the manipulation of the free parameters (μ , a , b , and c) allowing for different formations. For example, if $a = 1$, $b = 0$, and $c = 0$, then a ring formation that is parallel to the y - z plane is obtained. In the case of $a = 0$, $b = 0$, and $c = 0$, each UAV will be driven to distance r in the x - y - z plane, thus creating an sphere pattern.

As an example, consider a simplified formation of 10 point-mass UAVs that are desired to form three different formation patterns traveling at a constant speed u_x , once in their desired formation. To achieve this, the velocity field acting on each UAV is defined as

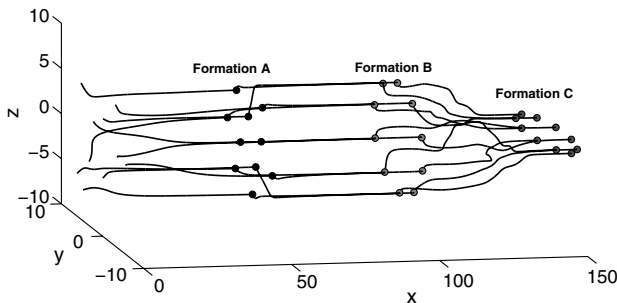


Fig. 12 Formation trajectory.

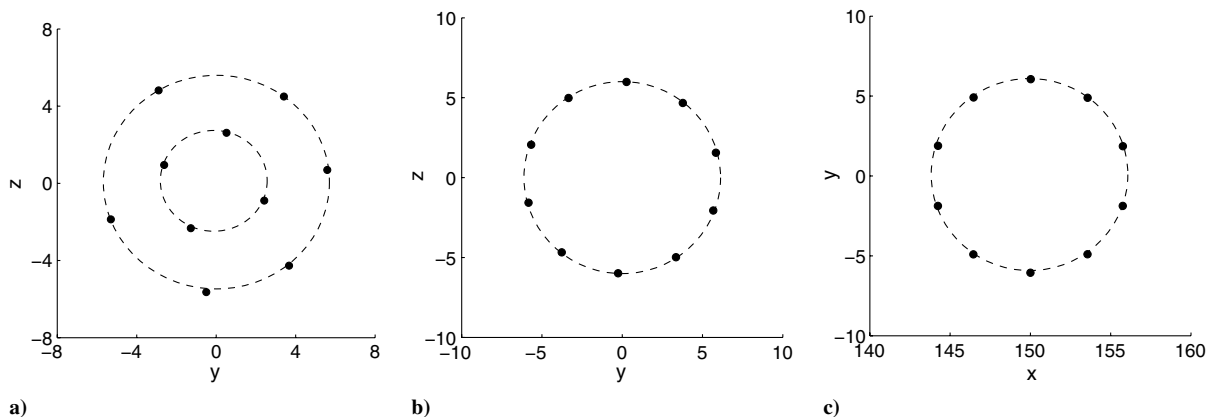


Fig. 13 Formation patterns: a) double-ring formation (radius = $r \pm \sqrt{\mu} = 2.6, 5.4$), b) single ring (radius = $r = 6$), and c) single ring (radius = $r = 6$).

$$\dot{\mathbf{x}}_i = 2\mu \frac{C_e}{L_e} \hat{\mathbf{x}}_i (|\mathbf{x}_i| - r) \exp^{-[(|\mathbf{x}_i| - r)^2 / L_e]} - C_h \left[\frac{\mathbf{k} \sigma_n}{(\sigma_n^2 + 1)^{0.5}} + \hat{\mathbf{x}}_n \frac{(|\mathbf{x}_n| - r)}{[(|\mathbf{x}_n| - r)^2 + 1]^{0.5}} \right] + \sum_{j, j \neq i} \frac{C_r}{L_r} \hat{\mathbf{x}}_{ij} \exp^{-|\mathbf{x}_{ij}| / L_r} + \mathbf{u}_c \quad (18)$$

where $x_n = x_i - u_x t$, t is time, $\mathbf{x}_n = (x_n, y_i, z_i)^T$, $\sigma_n = \mathbf{k} \cdot \mathbf{x}_n$, and $\mathbf{u}_c = (u_x, 0, 0)^T$.

The swarm of agents are desired to form a double-ring pattern in the y - z plane, which then bifurcates into a single-ring pattern and then a ring pattern in the x - y plane (radius = r). Each UAV is given random initial conditions, with a maximum speed of 5 and minimum separation distance of 1. It is also assumed that they can move instantaneously in all degrees of freedom and communicate freely with each other. The free parameters are chosen to satisfy these constraints, as summarized in Table 1.

Figures 12–15 show the formation trajectories, patterns, velocity profile, and separation distance. As can be seen, the swarm of agents autonomously forms the desired patterns, traveling at the desired speed once in equilibrium, and satisfies constraints made regarding the maximum speed and minimum separation distance between agents. It should be noted that, in the formation of the double ring, the split of UAVs is largely uncontrolled and dependent upon the initial conditions.

IV. Unmanned-Aerial-Vehicle Guidance and Control

A. Guidance Law

The desired velocity field is now transformed into a set of real commands for each UAV for desired forward speed (u_d), heading (ψ_d), and pitch (θ_d) as follows:

$$u_{d,i} = \sqrt{v_{x,i}^2 + v_{y,i}^2 + v_{z,i}^2} \quad (19)$$

$$\psi_{d,i} = \arctan\left(\frac{v_{y,i}}{v_{x,i}}\right) \quad (20)$$

$$\theta_{d,i} = \arctan\left(\frac{v_{z,i}}{v_{x,i}}\right) \quad (21)$$

Using these desired guidance commands, the new bound potential model is verified in a 6-DOF linear kinematic UAV model for a low-speed fixed-wing UAV that is linearized about straight and level flight conditions with a nominal forward speed of 11.3 ms^{-1} [27]. Equations (22) and (23) show the uncoupled longitudinal and lateral equations of motion, respectively, [28]

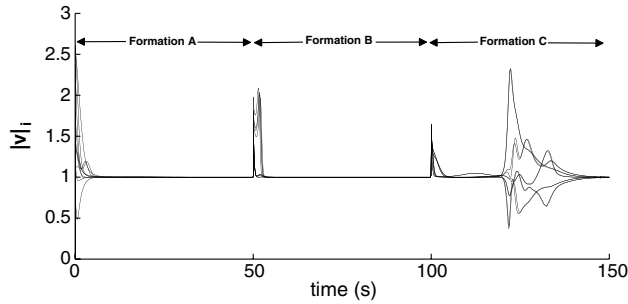


Fig. 14 Velocity profile of each agent.

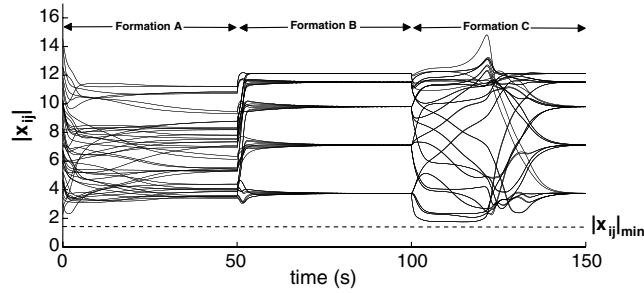


Fig. 15 Separation distance between agents.

$$\begin{bmatrix} \dot{u} \\ \dot{w} \\ \dot{q} \\ \dot{\theta} \\ \dot{\delta}_e \\ \dot{\delta}_r \end{bmatrix} = \begin{bmatrix} X_u & X_w & 0 & -g \cos \theta_0 & 0 & 0 \\ Z_u & Z_w & u_0 + z_q & -g \sin \theta_0 & 0 & 0 \\ M_u & M_w & M_q & 0 & 0 & 0 \\ 0 & 0 & 1 & 0 & 0 & 0 \\ 0 & 0 & 0 & 0 & -\frac{1}{T_e} & 0 \\ 0 & 0 & 0 & 0 & 0 & -\frac{1}{T_r} \end{bmatrix} \begin{bmatrix} u \\ w \\ q \\ \theta \\ \delta_e \\ \delta_r \end{bmatrix}$$

$$+ \begin{bmatrix} X_{\delta_e} & X_{\delta_r} \\ Z_{\delta_e} & Z_{\delta_r} \\ M_{\delta_e} & M_{\delta_r} \\ 0 & 0 \\ -\frac{1}{T_e} & 0 \\ 0 & -\frac{1}{T_r} \end{bmatrix} \begin{bmatrix} \delta_{e,d} \\ \delta_{r,d} \end{bmatrix} \quad (22)$$

$$\begin{bmatrix} \dot{v} \\ \dot{p} \\ \dot{r} \\ \dot{\phi} \\ \dot{\psi} \\ \dot{\delta}_a \\ \dot{\delta}_r \end{bmatrix} = \begin{bmatrix} Y_v & Y_p & Y_r - u_0 & g \cos \theta_0 & 0 & 0 & 0 \\ L_v & L_p & L_r & 0 & 0 & 0 & 0 \\ N_v & N_p & N_r & 0 & 0 & 0 & 0 \\ 0 & 1 & \tan \theta_0 & 0 & 0 & 0 & 0 \\ 0 & 0 & 1 & 0 & 0 & 0 & 0 \\ 0 & 0 & 0 & 0 & 0 & -\frac{1}{T_a} & 0 \\ 0 & 0 & 0 & 0 & 0 & 0 & -\frac{1}{T_r} \end{bmatrix} \begin{bmatrix} v \\ p \\ r \\ \phi \\ \psi \\ \delta_a \\ \delta_r \end{bmatrix}$$

$$+ \begin{bmatrix} Y_{\delta_a} & Y_{\delta_r} \\ L_{\delta_a} & L_{\delta_r} \\ N_{\delta_a} & N_{\delta_r} \\ 0 & 0 \\ 0 & 0 \\ -\frac{1}{T_a} & 0 \\ 0 & -\frac{1}{T_r} \end{bmatrix} \begin{bmatrix} \delta_{a,d} \\ \delta_{r,d} \end{bmatrix} \quad (23)$$

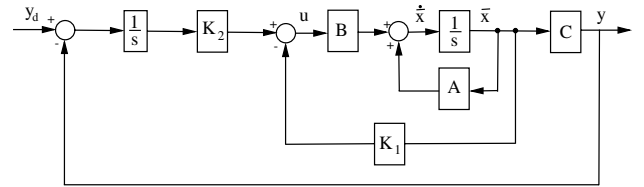


Fig. 16 Robust multivariable linear time-invariant control system.

where $(u, v, w)^T$ represent the forward, side, and vertical velocities, $(\phi, \theta, \psi)^T$ represent the roll, pitch, and yaw angles, $(p, q, r)^T$ represent the roll, pitch, and yaw rates, respectively, and $(\delta_a, \delta_r, \delta_e, \delta_r)^T$ and $(\delta_{a,d}, \delta_{r,d}, \delta_{e,d}, \delta_{r,d})^T$ represent the actual and desired aileron, rudder, and elevator deflections and thrust offsets, respectively. These state variables represent the deviation from the trim flight conditions. The stability derivatives for both longitudinal and lateral motions are given in [28].

B. Control Law

Both the longitudinal and lateral equations of motion can be expressed in the state-space form as

$$\dot{\bar{\mathbf{x}}} = \mathbf{A}\bar{\mathbf{x}} + \mathbf{B}\mathbf{u} = \mathbf{A} \begin{bmatrix} \bar{\mathbf{x}}_{\text{long}} \\ \bar{\mathbf{x}}_{\text{lat}} \end{bmatrix} + \mathbf{B} \begin{bmatrix} \mathbf{u}_{\text{long}} \\ \mathbf{u}_{\text{lat}} \end{bmatrix} \quad (24)$$

$$\mathbf{y} = \mathbf{C}\bar{\mathbf{x}} = \mathbf{C} \begin{bmatrix} \bar{\mathbf{x}}_{\text{long}} \\ \bar{\mathbf{x}}_{\text{lat}} \end{bmatrix} \quad (25)$$

where $\bar{\mathbf{x}}_{\text{long}} = [u, w, q, \theta, \delta_e, \delta_r]^T$ and $\bar{\mathbf{x}}_{\text{lat}} = [v, p, r, \phi, \psi, \delta_a, \delta_r]^T$ are the state variables of the system, $\mathbf{u}_{\text{long}} = [\delta_{e,d}, \delta_{r,d}]^T$ and $\mathbf{u}_{\text{lat}} = [\delta_{a,d}, \delta_{r,d}]^T$ are the inputs, and \mathbf{y} is the output of the system.

To achieve steady-state flight, consider the use of a robust controller of a linear time-invariant multivariable system [29]. First, the error \mathbf{e} in the system is defined as

$$\mathbf{e}(t) = \mathbf{y} - \mathbf{y}_d \quad (26)$$

where \mathbf{y}_d is the input to the system, as defined in Fig. 16.

Differentiating Eqs. (24) and (25) and assuming that, in steady state, $\dot{\mathbf{y}}_d = 0$, then

$$\frac{d}{dt} \dot{\bar{\mathbf{x}}} = \mathbf{A}\dot{\bar{\mathbf{x}}} + \mathbf{B}\dot{\mathbf{u}} \quad (27)$$

$$\frac{d}{dt} \mathbf{e} = \mathbf{C}\dot{\bar{\mathbf{x}}} \quad (28)$$

Combining Eqs. (27) and (28) results in

$$\frac{d}{dt} \begin{bmatrix} \dot{\bar{\mathbf{x}}}(t) \\ \mathbf{e}(t) \end{bmatrix} = \begin{bmatrix} \mathbf{A} & \mathbf{0} \\ \mathbf{C} & \mathbf{0} \end{bmatrix} \begin{bmatrix} \dot{\bar{\mathbf{x}}}(t) \\ \mathbf{e}(t) \end{bmatrix} + \begin{bmatrix} \mathbf{B} \\ \mathbf{0} \end{bmatrix} \dot{\mathbf{u}}(t) \quad (29)$$

To successfully control this system, the rank of Eq. (30) must be considered for controllability [28]:

$$\text{rank} \begin{bmatrix} \mathbf{A} & \mathbf{B} \\ \mathbf{C} & \mathbf{0} \end{bmatrix} = n + p \quad (30)$$

where n is the order of the \mathbf{A} matrix, and p is the order of the \mathbf{C} matrix.

Accordingly, it is found that only two state variables for both the longitudinal and lateral equations of motion can be controlled.

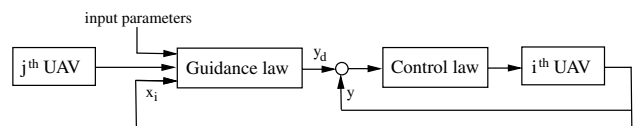


Fig. 17 Guidance and control block diagram.

Table 2 Static bifurcation free parameters

Time, s	μ	r	C_r	L_r	C_h	C_e	L_e	a	b	c
0–100	1	8	10	1.8	1	5	9	0	0	1
100–200	0	8	10	1.8	1	5	9	0	0	1
200–300	0	8	10	1.8	1	5	9	1	0	0

Therefore, controlling both forward speed and attitude and meeting the requirements of guidance algorithm, u and θ are chosen for longitudinal motion control, with v ($v = 0$ to control side slip) and ψ chosen for lateral motion control.

The input \mathbf{u} for both longitudinal and lateral motions of the controller is

$$\mathbf{u}(t) = -\mathbf{K}_1 \bar{\mathbf{x}}(t) - \mathbf{K}_2 \int_0^t \mathbf{e}(t) dt \quad (31)$$

where \mathbf{K}_1 and \mathbf{K}_2 are feedback gains of the controller, selected using the pole placement method [28,30].

It should be noted that if the system is in transition, \mathbf{y}_d is not constant. However, the system can still be controlled toward \mathbf{y}_d , as the poles of the system never change.

C. Numerical Simulation

Figure 17 shows the block diagram of the entire system using the proposed guidance and control laws.

Consider a formation of nine UAVs that are desired to transition between three patterns traveling at a constant final desired speed of 11.3 ms^{-1} (V_{trim}), assuming there is no wind. It will be assumed that the maximum speed each UAV can travel at is 15.1 ms^{-1} (V_{max}) and that the minimum separation distance between the UAVs is 2 m. As the UAV dynamics are linearized about trim flight conditions, the desired velocity field should be chosen such that $|\dot{\mathbf{x}}_d|_{\text{max}} \leq V_{\text{max}} - V_{\text{trim}}$. Therefore, from Eq. (14), it can be seen that

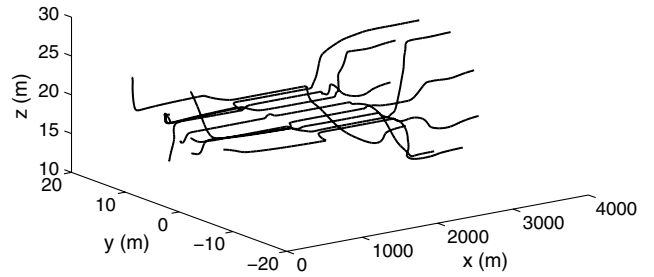


Fig. 19 Flight trajectories.

$$|\nabla U^S(\mathbf{x}_i)|_{\text{max}} = \lim_{|\mathbf{x}_i| \rightarrow \infty} |\nabla U^S(\mathbf{x}_i)| = 2C_h \quad (32)$$

From Eq. (2), the maximum gradient of the repulsive potential is

$$|\nabla U^R(\mathbf{x}_i)|_{\text{max}} = |\dot{\mathbf{x}}_d|_{\text{max}} - 2Ch \quad (33)$$

Knowing the desired minimum separation distance, C_r can be chosen as follows:

$$C_r = L_r \frac{|\dot{\mathbf{x}}_d|_{\text{max}} - 2Ch}{\exp^{-(|\mathbf{x}_{ij}|_{\text{min}}/L_r)}} \quad (34)$$

Table 2 summarizes the input parameters that were chosen to satisfy the constraints such that the UAVs will create a double-ring pattern and then bifurcate into an equally spaced ring pattern in the y - x plane and then the y - z plane.

The results of the simulation are shown in Figs. 18–23. Figures 18 and 19 show the formation patterns and flight trajectory. Figures 20 and 21 indicate that the simulation satisfies the constraints made regarding the maximum desired forward speed ($|\dot{\mathbf{x}}_d| \leq 3.8 \text{ ms}^{-1}$) and separation distance ($|\mathbf{x}_{ij}|_{\text{min}} = 2 \text{ m}$). Figures 22 show time histories of the state variables for an example UAV. The saturation limits of the aircraft control surfaces are $\delta_r \pm 30^\circ$, $\delta_a, \delta_e = \pm 25^\circ$, and

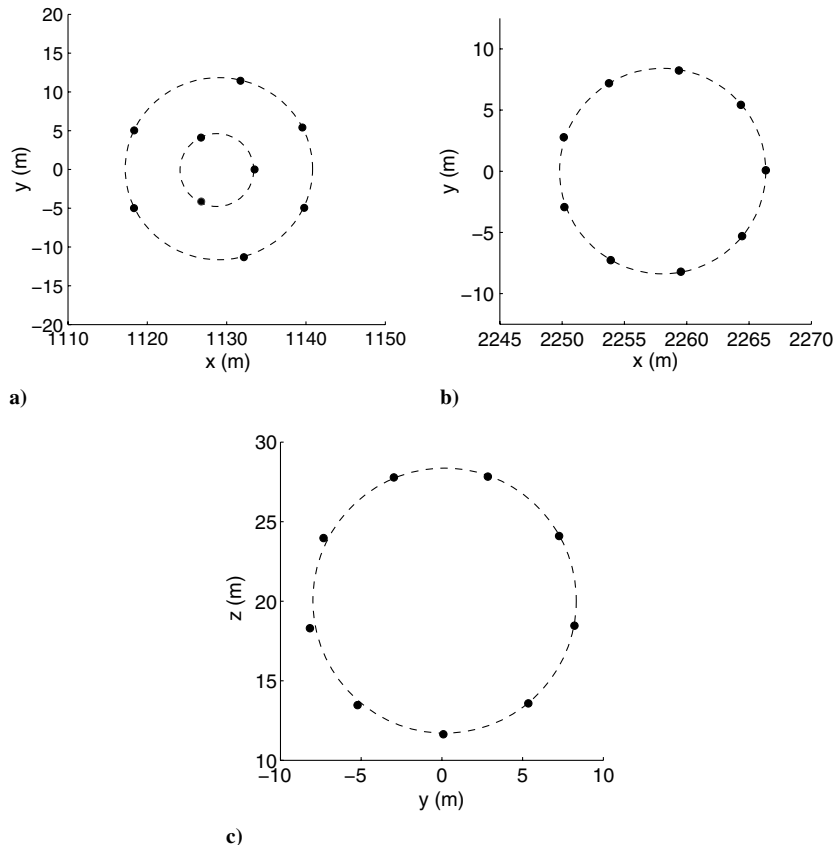


Fig. 18 UAV formations: a) pattern A, b) pattern B, and c) pattern C.

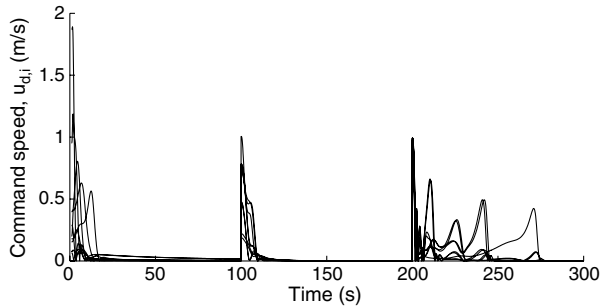


Fig. 20 Desired commanded forward speed.

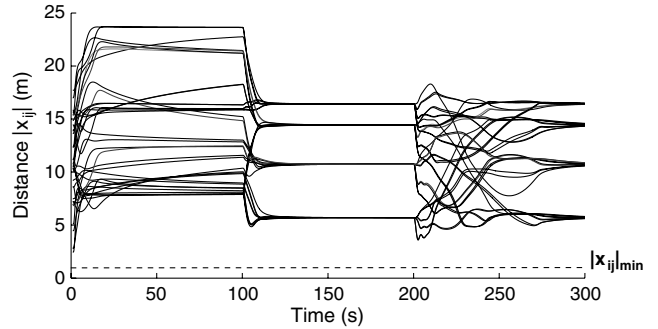


Fig. 21 Separation distance between UAVs.

thrust $\delta_i = \pm 1.5$ N, so the system can operate within these limits. Finally, Fig. 23 shows the time response of the controlled states on an example UAV. The results reveal that the UAV can follow the commands satisfactorily.

From the results shown, it can be seen that a formation of UAVs can safely form different patterns, satisfying the assumptions made

regarding each UAV. The purpose of this section was to demonstrate that the new methodology could be applied as a guidance algorithm for a swarm of UAVs. As such, a simplified model of a UAV was considered. This can be improved further by considering higher-order models of the UAV kinematics, for example. In addition, when

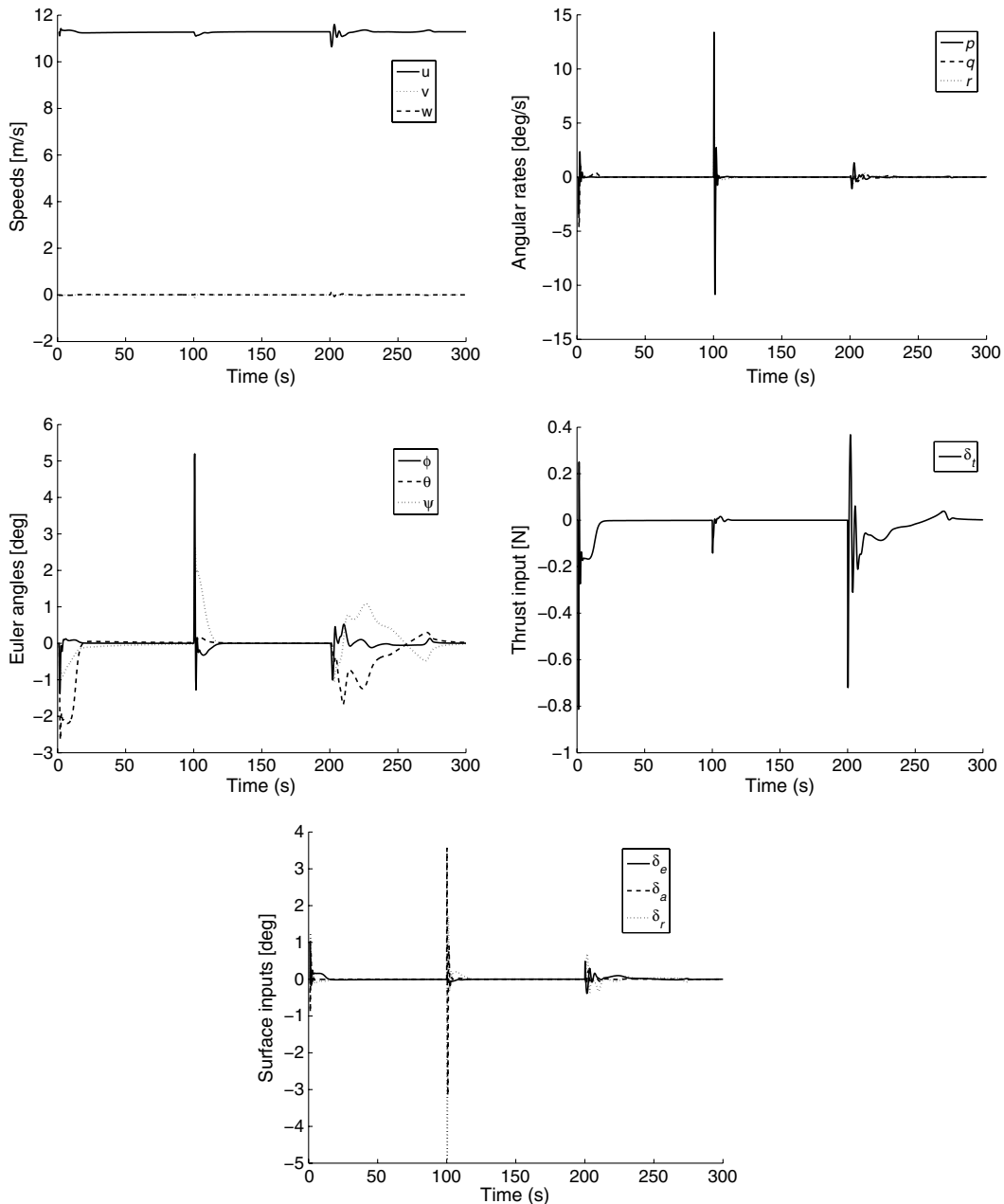


Fig. 22 Time histories of speed, angular rate, Euler angles, and inputs (UAV 1).

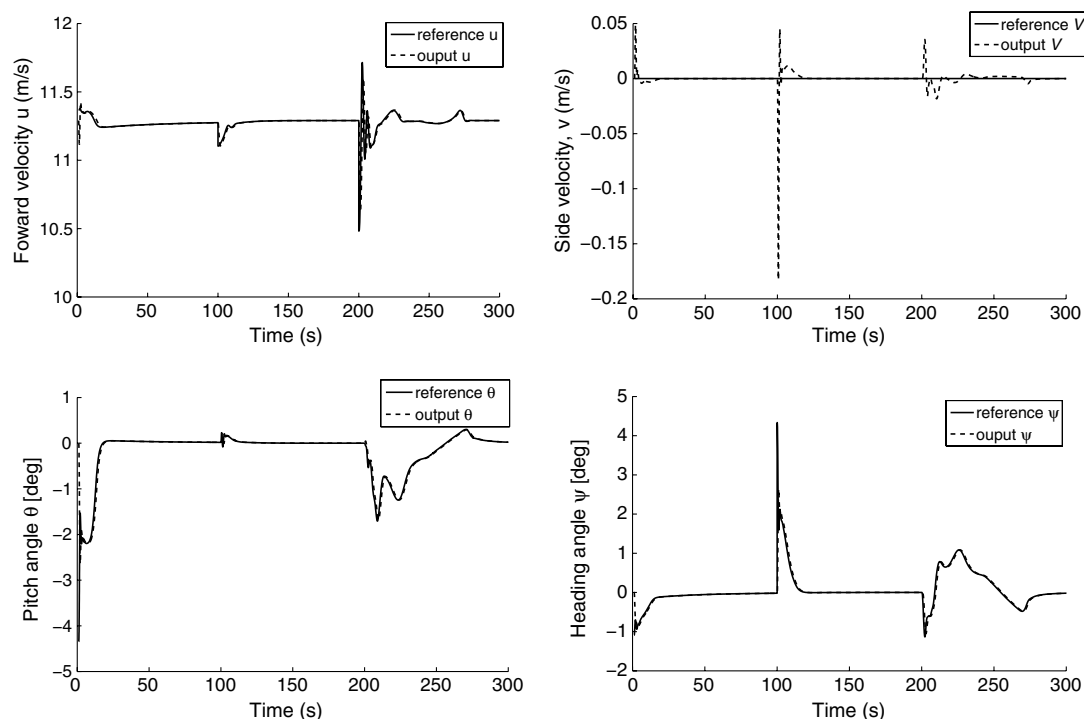


Fig. 23 Time histories of controlled states (UAV 1).

simulating the UAV system, all aspects of the UAV dynamics could be considered. This may include the UAV structure, propulsion system, sensors, and consideration of the atmospheric flight conditions [31]. For example, an important perturbation when dealing with small UAVs is to consider the effect of wind on the system. Another assumption made was that the communication system was ideal. As Sigurd and How point out, although the APF method is theoretically elegant, the assumption that all UAVs have information on all other UAVs is unrealistic, as the number of UAVs increases [32]. Related work has attempted to address this issue by assuming each UAV will have a sensing region surrounding them as opposed to the requirement for global knowledge [23]. It is shown that a scale separation exists between each UAV such that it moves under the influence of a long-range steering potential with short-range collision avoidance so that the assumption of a sensing region could be considered valid. Although not a rigorous proof, Tanner et al. has shown that, by using graph theory, if the communication network between the UAVs remains connected for all time, the system is guaranteed to relax into the minimum of the potential [33]. Another area of future work is the sizing of the repulsive potential to ensure that the minimum separation distance between the UAVs is larger than the physical dimensions. This has been considered in [23], where it was estimated that minimum separation distance between the UAVs is dependent upon the maximum velocity of the UAV and constants chosen in the repulsive potential field. Therefore, as discussed, there is scope for further improvement, and all points considered can be viewed as part of future work.

V. Conclusions

This paper has considered a new bounded guidance law for a swarm of UAVs. Based on the new approach of bifurcating APFs, it is shown that a formation of UAVs can be successfully controlled such that verifiable, autonomous patterns are achieved, with a simple parameter switch allowing for the transition between patterns. In real safety-critical applications, it is important to ensure that the vehicle actuators are not saturated. As such, a new bounded bifurcating potential field is developed and translated into a set of guidance commands that control speed, heading, and pitch angle. To demonstrate the method, the guidance law is implemented in a linearized 6-DOF fixed-wing UAV model for nine UAVs, controlled using a

robust multisteady state variable linear time-invariant control system. The results show that the swarm of UAVs can successfully form patterns, switching autonomously between them through a simple parameter switch to the potential, satisfying constraints made regarding each UAV. To further improve the model, several assumptions made regarding the system will be considered in the future. For example, it was assumed that the communication system between the UAVs was ideal. Future work will consider the implementation of a sensing region surrounding each UAV and its influence on the stability of the swarm. In addition, it was assumed that there were no external perturbations acting on each UAV and all sensors were ideal. The development of a control law to take this into consideration will also be investigated.

References

- [1] Pamphile, T., and Lin, Kuo-Chi, "Behavior-Based Control Hierarchy of Unmanned Aerial Vehicle Swarming," *International Symposium on Collaborative Technologies and Systems, 2006 (CTS 2006)*, IEEE Computer Soc., Washington, D.C., May 2006, pp. 349–355.
- [2] Gu, Y., Seanor, B., Campa, G., Napolitano, M. R., Rowe, L., Gururanjan, S., and Wan, S., "Design of Flight Testing Evaluation of Formation Control Laws," *IEEE Transactions on Control Systems Technology*, Vol. 14, No. 6, 2006, pp. 1105–1112. doi:10.1109/TCST.2006.880203
- [3] Ryoo, C. K., Kim, Y. H., and Tahk, M. J., "Formation Guidance Laws with Timing Constraint," *International Journal of Systems Science*, Vol. 37, No. 6, 2006, pp. 415–427. doi:10.1080/00207720500438340
- [4] Kim, S., and Kim, Y., "Three Dimensional Optimum Controller for Multiple UAV Formation Flight Using Behavior-Based Decentralized Approach," *International Conference on Control, Automation and Systems, ICROS*, Seoul, Oct. 2007, pp. 1387–1392.
- [5] Lee, J., Kim, H. S., Kim, Y., and Han, K., "Formation Geometry Center Based Formation Controller Design Using Lyapunov Stability Theorem," *International Journal of Aeronautical and Space Sciences*, Vol. 9, No. 2, 2008, pp. 71–78. doi:10.5139/IJASS.2008.9.2.071
- [6] Paul, T., Krogstad, T. R., and Gravdahl, J. T., "Modeling of UAV Formation Flight Using 3D Potential Field," *Simulation Modelling Practice and Theory*, Vol. 16, No. 9, 2008, pp. 1453–1462. doi:10.1016/j.simpat.2008.08.005
- [7] Bonabeau, E., Dorigo, M., and Theraulaz, G., *Swarm Intelligence: From Natural to Artificial Systems*, Oxford, New York, 1999, p. 7.

- [8] Reynolds, C., "Flocks, Herds and Schools: A Distributed Behavioural Model," *Computer Graphics*, Vol. 21, No. 4, 1987, pp. 25–34. doi:10.1145/37402.37406
- [9] Heppner, F., and Grenander, U., "A Stochastic Non-Linear Model for Coordinated Bird Flocks," *The Ubiquity of Chaos*, edited by S. Krasner, AAAS Publ., Washington, D.C., 1990, pp. 233–238.
- [10] Crowther, W. J., "Flocking of Autonomous Unmanned Air Vehicles," *The Aeronautical Journal*, Vol. 107, No. 1068, 2003, pp. 99–110.
- [11] Crowther, W. J., "Rule-Based Guidance for Flight Vehicle Flocking," *Proceedings of the Institution of Mechanical Engineers, Part G: Journal of Aerospace Engineering*, Vol. 218, No. 2, 2004, pp. 111–124. doi:10.1243/0954410041322005
- [12] Brooks, R. A., "A Robust Layered Control System for a Mobile Robot," *IEEE Journal of Robotics and Automation*, Vol. 2, No. 1, 1986, pp. 14–23. doi:10.1109/JRA.1986.1087032
- [13] Warren, C. W., "Global Path Planning Using Artificial Potential Fields," *Proceedings of the 1989 IEEE International Conference on Robotics and Automation*, Vol. 1, IEEE Publ., Piscataway, NJ, May 1989, pp. 316–321.
- [14] Khatib, O., "Real-Time Obstacle Avoidance for Manipulators and Mobile Robots," *International Journal of Robotics Research*, Vol. 5, No. 1, 1986, pp. 90–98. doi:10.1177/027836498600500106
- [15] Volpe, R., and Khosla, P., "Manipulator Control with Superquadric Artificial Potential Functions: Theory and Experiments," *IEEE Transactions on Systems, Man, and Cybernetics*, Vol. 20, No. 6, Nov.–Dec. 1990, pp. 1423–1436. doi:10.1109/21.61211
- [16] Ge, S. S., and Cui, Y. J., "Dynamic Motion Planning for Mobile Robots Using Potential Field Method," *Autonomous Robots*, Vol. 13, No. 3, 2002, pp. 207–222. doi:10.1023/A:1020564024509
- [17] Nguyen, B. Q., Chuang, Y.-L., Tung, D., Hsieh, C., Jin, Z., Shi, L., Marthaler, D., Bertozzi, A., and Murray, R. M., "Virtual Attractive-Repulsive Potentials for Cooperative Control of Second Order Dynamic Vehicles on the Caltech MVWT," *American Control Conference*, Vol. 2, IEEE Publ., Piscataway, NJ, June 2005, pp. 1084–1089.
- [18] Huang, W. H., Fajen, B. R., Fink, J. R., and Warren, W. H., "Visual Navigation and Obstacle Avoidance Using a Steering Potential Function," *Robotics and Autonomous Systems*, Vol. 54, No. 4, 2006, pp. 288–299. doi:10.1016/j.robot.2005.11.004
- [19] Reif, J. H., and Wang, H., "Social Potential Fields: A Distributed Behavioral Control for Autonomous Robots," *Robotics and Autonomous Systems*, Vol. 27, No. 3, 1999, pp. 171–194. doi:10.1016/S0921-8890(99)00004-4
- [20] Chang, D. E., Shadden, S. C., Marsden, J. E., and Olfati-Saber, R., "Collision Avoidance for Multiple Agent Systems," *Proceedings of the 42nd IEEE Conference on Decision and Control*, Vol. 1, IEEE Publ., Piscataway, NJ, Dec. 2003, pp. 539–543.
- [21] Ogren, P., Fiorelli, E., and Leonard, N. E., "Cooperative Control of Mobile Sensor Networks: Adaptive Gradient Climbing in a Distributed Environment," *IEEE Transactions on Automatic Control*, Vol. 49, No. 8, 2004, pp. 1292–1302. doi:10.1109/TAC.2004.832203
- [22] D'Orsogna, M. R., Chuang, Y. L., Bertozzi, A. L., and Chayes, S., "Self-Propelled Particles with Soft-Core Interactions: Patterns, Stability, and Collapse," *Physical Review Letters*, Vol. 96, No. 10, March 2006, Paper 104302.
- [23] Bennet, D. J., and McInnes, C. R., "Verifiable Control of a Swarm of Unmanned Aerial Vehicles," *Proceedings of the Institution of Mechanical Engineers, Part G: Journal of Aerospace Engineering*, Vol. 223, No. 7, 2009, pp. 939–953. doi:10.1243/09544100JAERO508
- [24] Frew, E., Lawrence, D. A., and Morris, S., "Coordinated Standoff Tracking of Moving Targets Using Lyapunov Guidance Vector Fields," *Journal of Guidance, Control, and Dynamics*, Vol. 31, No. 2, March–April 2008, pp. 290–306. doi:10.2514/1.30507
- [25] Han, K., Lee, J., and Kim, Y., "Unmanned Aerial Vehicle Swarming Control Using Potential Functions and Sliding Mode Control," *Proceedings of the Institution of Mechanical Engineers, Part G: Journal of Aerospace Engineering*, Vol. 222, No. 6, 2008, pp. 721–730. doi:10.1243/09544100JAERO352
- [26] Badawy, A., and McInnes, C. R., "Robot Motion Planning Using Hyperboloid Potential Functions," *World Congress on Engineering*, London, July 2007, pp. 1231–1235.
- [27] Hyslop, A. M., and Humbert, J. S., "Wide-Field Integration Methods for Autonomous Navigation in 3-D Environments," AIAA Guidance, Navigation and Control Conference and Exhibit, Honolulu, HI, AIAA Paper 2008-7252, Aug. 2008.
- [28] Kokume, M., and Uchiyama, K., "Guidance Law Based on Bifurcating Velocity Field for Formation Flight," AIAA Guidance, Navigation, and Control Conference, Toronto, AIAA Paper 2010-8081, Aug. 2010.
- [29] Davison, E., "The Robust Control of a Servomechanism Problem for Linear Time-Invariant Multivariable Systems," *IEEE Transactions on Automatic Control*, Vol. 21, No. 1, 1976, pp. 25–34. doi:10.1109/TAC.1976.1101137
- [30] Suzuki, M., and Uchiyama, K., "Autonomous Formation Flight Using Bifurcating Potential Fields," *27th Congress of the International Council of the Aeronautical Sciences*, Nice, France, Sept. 2010, pp. 1–8.
- [31] Sadraey, M., and Colgren, R., "UAV Flight Simulation: Credibility of Linear Decoupled vs. Nonlinear Coupled Equations of Motion," AIAA Modeling and Simulation Technologies Conference and Exhibit, San Francisco, CA, AIAA Paper 2005-6425, Aug. 2005.
- [32] Sigurd, K., and How, J., "UAV Trajectory Design Using Total Field Collision Avoidance," AIAA Guidance, Navigation and Control Conference, AIAA Paper 2003-5728, Aug. 2003.
- [33] Tanner, H. G., Jadabaie, A., and Pappas, G. J., "Flocking in Fixed and Switching Networks," *IEEE Transactions on Automatic Control*, Vol. 52, No. 5, 2007, pp. 863–868. doi:10.1109/TAC.2007.895948